Article

A Numerical Solution of Symmetric Angle Ply Plates Using Higher-Order Shear Deformation Theory

Saira Javed

Department of Mathematics and Statistics, College of Science, King Faisal University,
P.O. Box 400, Al Ahsa 31982, Saudi Arabia; sulhaque@kfu.edu.sa

Abstract: This research aims to provide the numerical analysis solution of symmetric angle ply plates using higher-order shear deformation theory (HSDT). The vibration of symmetric angle ply composite plates is analyzed using differential equations consisting of supplanting and turning functions. These supplanting and turning functions are numerically approximated through spline approximation. The obtained global eigenvalue problem is solved numerically to find the eigenfrequency parameter and a related eigenvector of spline coefficients. The plates of different constituent components are used to study the parametric effects of the plate's aspect ratio, side-to-thickness ratio, assembling sequence, number of composite layers, and alignment of each layer on the frequency of the plate. The obtained results are validated by existing literature.

Keywords: composite plates; numerical analysis solution; HSDT; symmetric angle ply; eigenfrequency parameter

1. Introduction

The research aims to provide a numerical analysis solution for symmetric angle ply plates using HSDT. The vibration of symmetric angle ply composite plates is analyzed using supplanting and turning functions, which are numerically approximated by spline approximation. Laminated plates have widely been used in many engineering fields and engineering structures because of their ability to alter mechanical properties. Additionally, the composite plates offer higher stiffness-to-weight ratios, strength-to-weight ratios, and shock-absorbing features than the homogeneous plates. One of the benefits of using composite plates leads to designing such structures which have maximum reliability and minimum weight. Layered plates show larger thickness effects than plates made of homogeneous materials, which tend to study the free vibration of laminated composite plates under third-order shear deformation theory.

The classical theory (CT) is based on the Love–Kirchhoff assumption. In this theory, the lines which are normal to the undeformed and deformed mid-plane remain straight and normal and do not experience any stretching along the z direction. The stress of thin composite plates can be precisely calculated by CT. However, it is not appropriate for thick laminated plates because the natural frequencies are overestimated (Vinson [1]; Noor and Burton [2]). So, in order to study relatively thick plates, the effect of shear deformation should be taken into account. Yang, Nooris, and Stavsky [3] developed the first-order shear deformation theory (FSDT) which states that there is constant shear strain through the z direction of the plate (transverse shear strain). Moreover, there are different higher-order plate theories to precisely calculate the transverse shear stresses which effectively occurs in thick plates. In higher-order plate theories, the displacements are extended to any desired degree in terms of thickness coordinates (Vinson [1] Noor and Burton [2]). In third-order plate theory, the displacement functions are extended to the terms with the power of three in thickness coordinates to have a quadratic variation of transverse shear strains and transverse shear stresses through the plate thickness. This avoids the need for

a shear correction coefficient (Reddy [4]). The third-order plate TSDT theory by Reddy is widely used because it can represent transverse shear stresses in an efficient way.

Ghiamy and Amoushahi [5] investigated the stability of sandwich plates using the third-order shear deformation theory. Free and forced vibrations of graphene-filled plates were analyzed by Parida and Jena [6]. Zhao et al. [7] used the Jacobi–Ritz approach to study annular plates based on a higher-order shear deformation theory. Tian et al. [8] studied the nonlinear stability of organic solar cells using the third-order shear deformation plate theory. Bending, free vibration, and buckling of FGM plates were analyzed under HSDT by Belkhodja [9]. Third-order shear deformation theory was analyzed on graphene nanoplates for the modified couple stress theory (Eskandari et al. [10]). Shi and Dong [11] used the refined hyperbolic shear deformation theory to analyze the laminated composite plates. Javani et al. [12] used the GDQE procedure to study the free vibration of FG-GPLRC folded plates. A new higher-order shear deformation theory was used to study the free vibration of sandwich-curved beams (Sayyad and Avhad [13]). Ellali et al. [14] investigated the thermal buckling of a sandwich beam attached to piezoelectric layers based on the shear deformation theory. Bending, free vibration, and buckling analysis of functionally graded porous beams were examined using the shear deformation theory by Nguyen et al. [15]. Peng et al. [16] used the MK method to study static and free vibration analysis of stiffened FGM plates. Free vibration of functionally graded porous non-uniform thickness annular nanoplates using the ES-MITC3 element was studied by Pham et al. [17]. Hung et al. [18] used the modified strain gradient theory to analyze refined isogeometric plates. Sharma et al. [19] investigated the static and free vibration of smart variable stiffness laminated composite plates. Cho [20] examined the nonlinear free vibration of functionally graded CNT-reinforced plates. Functionally graded plates were studied for their static and free vibration by Zang et al. [21]. Ghosh and Haldar [22] analyzed the free vibration of laminated composite plates on elastic point supports using the finite element method. The extended Ritz method was used to analyze the free vibrations of cracked variable stiffness composite plates by Milazzo [23]. Saiah et al. [24] studied the free vibration behavior of nanocomposite laminated plates containing functionally graded graphene-reinforced composite plies. Singh and Karathanasopoulos [25] examined the composite plates using an elasticity solution under the patch loads. Belardi et al. [26] investigated the Ritz method to analyze the bending and stress of sector plates. Zhong et al. [27] analyzed the laminated annular plate backed by double cylindrical acoustic cavities.

Several studies have been conducted to investigate the mechanical properties and behavior of composite materials, including alkali-activated composites (Wang et al. [28]), hierarchical cellular honeycombs (Zhang et al. [29]), welding residual stress distribution of corrugated steel webs (Zhang et al. [30]), and microcracking behavior of crystalline rock (Peng et al. [31]). However, to the best of our knowledge, there are limited studies that have investigated the parametric effects of the plate's aspect ratio, side-to-thickness ratio, assembling sequence, number of composite layers, and alignment of each layer on the frequency of symmetric angle ply plates.

This research utilizes differential equations in terms of displacement and rotational functions to analyze the vibration of symmetric angle ply composite plates. The spline approximation method is used to numerically approximate the displacement and rotational functions. The obtained spline coefficients are then used to solve a generalized eigenvalue problem numerically. The eigenvalue problem provides an eigenfrequency parameter and an associated eigenvector, which can be used to study the frequency response of the plate. The simply supported boundary condition is considered to analyze the geometric effects of the plate's aspect ratio, side-to-thickness ratio, assembling sequence, number of composite layers, and alignment of each layer on the frequency of the plate. Results are narrated by using graphs and tables.

2. Solution of Problem

A rectangular plate considered has the Cartesian coordinate system x, y, and z, with the x, y plane placed at mid-depth (reference surface) of the plate and z taken normal to the plate, as shown in Figure 1. Here, a and b are the lengths of the sides of the plate along the x and y directions, respectively, h is the total thickness, and h_k is the thickness of the k-th layer of the plate.
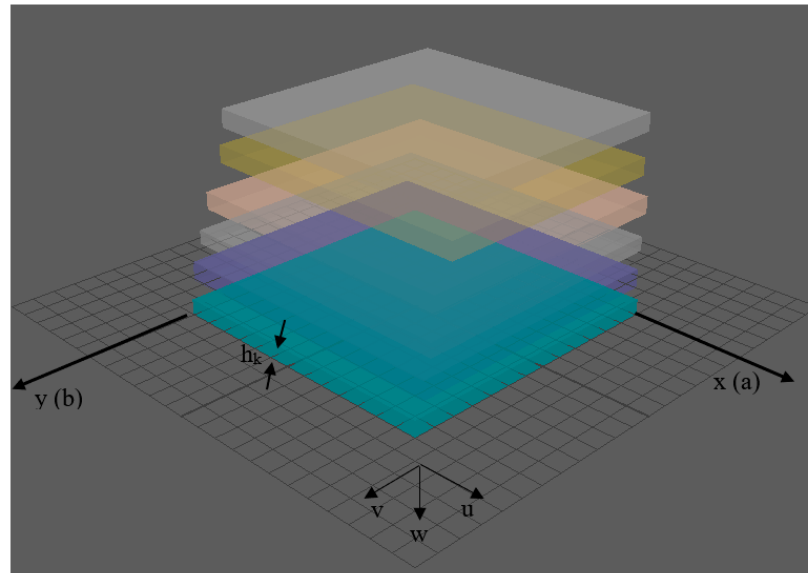

Figure 1. Composite plate geometry.

The following equilibrium equations are derived using the dynamic version of the principle of virtual displacements for the higher-order theory (Reddy [32]).

$$
\begin{aligned}
N_{x,x} + N_{xy,y} &= I_0\, u_{0\,tt} \\
N_{xy,x} + N_{y,y} &= I_0\, v_{0\,tt} \\
\overline{Q}_{x,x} + \overline{Q}_{y,y} + c_1\left(P_{x,xx} + 2P_{xy,xy} + P_{y,yy}\right) &= I_0\, w_{0\,tt} - c_1^2 I_6\left(w_{0\,xxtt} + w_{0\,yytt}\right) + c_1 J_4\left(\phi_{x,xtt} + \phi_{y,ytt}\right) \\
\overline{M}_{x,x} + \overline{M}_{xy,y} - \overline{Q}_x &= K_2\, \phi_{x,tt} - c_1 J_4\, w_{0\,xtt} \\
\overline{M}_{xy,x} + \overline{M}_{y,y} - \overline{Q}_y &= K_2\, \phi_{y,tt} - c_1 J_4\, w_{0\,ytt}
\end{aligned}
\tag{1}
$$

Equation (1) is an equilibrium equation in the dynamic form as it consists of force, moment, transverse shear force resultants, and inertia force components.

I_i are mass moments of inertia, which are defined as follows:

$I_i = \int_z \rho^{(k)}(z)^i dz \quad (i = 0, 1, 2, 3, \ldots, 6)$ and ρ is the material density of the k-th layer.

u, v, and w are the displacement components in the x, y, and z directions, respectively, u_0, v_0, and w_0 are the in-plane displacements of the middle plane, and ψ_x and ψ_y are the shear rotations of any point on the middle surface of the plate.

$$
\overline{M}_{\alpha\beta} = M_{\alpha\beta} - c_1 P_{\alpha\beta}, \qquad \overline{Q}_\alpha = Q_\alpha - c_2 R_\alpha
$$

$$
J_i = I_i - c_1 I_{i+2} \qquad K_2 = I_2 - 2c_1 I_4 + c_1^2 I_6
$$

where N_i, M_i, and Q_i are in-plane force resultant, moment resultant, and transverse shear force resultants, respectively. P_i and R_i denote higher-order stress resultants.

The stress resultants are defined as:

$$
\left\{\begin{array}{c} N_i \\ M_i \\ P_i \end{array}\right\} = \int_{-h/2}^{h/2} \sigma_i \left\{\begin{array}{c} 1 \\ z \\ z^3 \end{array}\right\} dz, \qquad \left\{\begin{array}{c} Q_i \\ R_i \end{array}\right\} = \int_{-h/2}^{h/2} \tau_i \left\{\begin{array}{c} 1 \\ z^2 \end{array}\right\} dz
\tag{2}
$$

The stress–strain relationships for the *k*-th layer, after neglecting transverse normal strain and stress, is of the form:

$$
\begin{pmatrix} \sigma_x^{(k)} \\ \sigma_y^{(k)} \\ \tau_{xy}^{(k)} \\ \tau_{yz}^{(k)} \\ \tau_{xz}^{(k)} \end{pmatrix} = \begin{pmatrix} Q_{11}^{(k)} & Q_{12}^{(k)} & Q_{16}^{(k)} & 0 & 0 \\ Q_{12}^{(k)} & Q_{22}^{(k)} & Q_{26}^{(k)} & 0 & 0 \\ Q_{16}^{(k)} & Q_{26}^{(k)} & Q_{66}^{(k)} & 0 & 0 \\ 0 & 0 & 0 & Q_{44}^{(k)} & Q_{45}^{(k)} \\ 0 & 0 & 0 & Q_{45}^{(k)} & Q_{55}^{(k)} \end{pmatrix} \begin{pmatrix} \varepsilon_x^{(k)} \\ \varepsilon_y^{(k)} \\ \gamma_{xy}^{(k)} \\ \gamma_{yz}^{(k)} \\ \gamma_{xz}^{(k)} \end{pmatrix}
\tag{3}
$$

where $Q_{ij}^{(k)}$ are elements of the stiffness matrix defined in Appendix A.

When the materials are oriented at an angle θ with the *x*-axis, the transformed stress–strain relationships are as follows:

$$
\begin{pmatrix} \sigma_x^{(k)} \\ \sigma_y^{(k)} \\ \tau_{xy}^{(k)} \\ \tau_{yz}^{(k)} \\ \tau_{yz}^{(k)} \end{pmatrix} = \begin{pmatrix} \overline{Q}_{11}^{(k)} & \overline{Q}_{12}^{(k)} & \overline{Q}_{16}^{(k)} & 0 & 0 \\ \overline{Q}_{12}^{(k)} & \overline{Q}_{22}^{(k)} & \overline{Q}_{26}^{(k)} & 0 & 0 \\ \overline{Q}_{16}^{(k)} & \overline{Q}_{26}^{(k)} & \overline{Q}_{66}^{(k)} & 0 & 0 \\ 0 & 0 & 0 & \overline{Q}_{44}^{(k)} & \overline{Q}_{45}^{(k)} \\ 0 & 0 & 0 & \overline{Q}_{45}^{(k)} & \overline{Q}_{55}^{(k)} \end{pmatrix} \begin{pmatrix} \varepsilon_x^{(k)} \\ \varepsilon_y^{(k)} \\ \gamma_{xy}^{(k)} \\ \gamma_{yz}^{(k)} \\ \gamma_{xz}^{(k)} \end{pmatrix}
\tag{4}
$$

where $\overline{Q}_{ij}^{(k)}$ are elements of the transformed stiffness matrix given in Appendix A.

In-plane strains are defined as:

$$
\varepsilon = \begin{Bmatrix} \varepsilon_x \\ \varepsilon_y \\ \gamma_{xy} \end{Bmatrix}; \qquad \varepsilon = \varepsilon^0 + z\varepsilon^1 + z^3\varepsilon^3
\tag{5}
$$

where:

$$
\varepsilon^0 = \begin{Bmatrix} \varepsilon_x^0 \\ \varepsilon_y^0 \\ \gamma_{xy}^0 \end{Bmatrix} = \begin{Bmatrix} u_{0\,x} \\ v_{0\,y} \\ u_{0\,y} + v_{0\,x} \end{Bmatrix}, \varepsilon^1 = \begin{Bmatrix} \varepsilon_x^1 \\ \varepsilon_y^1 \\ \gamma_{xy}^1 \end{Bmatrix} = \begin{Bmatrix} \phi_{x,x} \\ \phi_{y,y} \\ \phi_{x,y} + \phi_{y,x} \end{Bmatrix}, \varepsilon^3 = \begin{Bmatrix} \varepsilon_x^3 \\ \varepsilon_y^3 \\ \gamma_{xy}^3 \end{Bmatrix} = \left(-\frac{4}{3h^2}\right) \begin{Bmatrix} \phi_{x,x} + w_{0\,xx} \\ \phi_{y,y} + w_{0\,yy} \\ \phi_{x,y} + \phi_{y,x} + 2w_{0\,xy} \end{Bmatrix}
$$

The shear strain components are defined as:

$$
\gamma = \begin{Bmatrix} \gamma_{yz} \\ \gamma_{xz} \end{Bmatrix}; \qquad \gamma = \gamma^0 + z^2\gamma^2
\tag{6}
$$

where:

$$
\gamma^0 = \begin{Bmatrix} \gamma_{yz}^0 \\ \gamma_{xz}^0 \end{Bmatrix} = \begin{Bmatrix} \phi_y + w_{0\,y} \\ \phi_x + w_{0\,x} \end{Bmatrix}, \gamma^2 = \begin{Bmatrix} \gamma_{yz}^2 \\ \gamma_{xz}^2 \end{Bmatrix} = \left(-\frac{4}{h^2}\right) \begin{Bmatrix} \phi_y + w_{0\,y} \\ \phi_x + w_{0\,x} \end{Bmatrix}
$$

When any structure vibrates with a certain frequency, it causes stress and in return strain. Strain is the ratio of the change in length to the original length. Deformations that are applied perpendicular to the cross-section are normal strains (ε), while deformations applied parallel to the cross-section are shear strains (γ).

The stress–strain relationships are obtained as follows:

$$
\begin{pmatrix} N \\ M \\ P \\ Q \\ R \end{pmatrix} = \begin{pmatrix} A & 0 & 0 & 0 & 0 \\ 0 & D & F & 0 & 0 \\ 0 & F & H & 0 & 0 \\ 0 & 0 & 0 & A' & D' \\ 0 & 0 & 0 & D' & F' \end{pmatrix} \begin{pmatrix} \varepsilon^0 \\ \varepsilon^1 \\ \varepsilon^3 \\ \gamma^0 \\ \gamma^2 \end{pmatrix}
\tag{7}
$$

where N, M, Q, P, and R are obtained by integrating stress and strain components across the thickness of the plate. After integration, a modified equation in matrix form is written as Equation (7). Values of strain (ε) and shear strain (γ) component given in Equations (2)–(4) are inserted to the given system of the equation. After that, displacements and rotational functions given in Equation (9) are used and the resulting Equation (10) is obtained.

Stiffness coefficients are defined as:

$$A_{ij} = \sum_k Q_{ij}^{(k)}\left(z_k - z_{k-1}\right), \quad D_{ij} = \frac{1}{3}\sum_k Q_{ij}^{(k)}\left({z^3}_k - {z^3}_{k-1}\right),$$

$$F_{ij} = \frac{1}{5}\sum_k Q_{ij}^{(k)}\left({z^5}_k - {z^5}_{k-1}\right), \quad \text{For } i,j = 1,2,6,$$

$$A'_{ij} = \sum_k Q_{ij}^{(k)}\left(z_k - z_{k-1}\right), \quad D'_{ij} = \frac{1}{3}\sum_k Q_{ij}^{(k)}\left({z^3}_k - {z^3}_{k-1}\right) \text{ and } F'_{ij} = \frac{1}{5}\sum_k Q_{ij}^{(k)}\left({z^5}_k - {z^5}_{k-1}\right) \tag{8}$$

for $i,j = 4,5$.

Where the elastic coefficients A_{ij} and D_{ij} (extensional and bending stiffnesses) and F_{ij} and H_{ij} are the higher-order stiffness coefficients.

The supplanting and turning functions are assumed in the separable form for symmetric angle ply plates as cos and sine functions as follows:

$$\begin{aligned}
u(x,y) &= U(x)\cos\frac{n\pi y}{b}e^{i\omega t}\\
v(x,y) &= V(x)\sin\frac{n\pi y}{b}e^{i\omega t}\\
w(x,y) &= W(x)\sin\frac{n\pi y}{b}e^{i\omega t}\\
\psi_x(x,y) &= \Psi_x(x)\sin\frac{n\pi y}{b}e^{i\omega t}\\
\psi_y(x,y) &= \Psi_y(x)\cos\frac{n\pi y}{b}e^{i\omega t}
\end{aligned} \tag{9}$$

The non-dimensional parameters introduced are as follows:

$\lambda = \omega a\sqrt{\frac{I_0}{A_{11}}}$ is the frequency parameter and $\delta_k = \frac{h_k}{h}$ is the relative layer thickness of the k-th layer.

$\phi = \frac{a}{b}$ is the aspect ratio, $X = \frac{x}{a}$ is the distance co-ordinate, and $H = \frac{a}{h}$ is the side-to-thickness ratio.

Using cos and sine functions for displacements and rotational functions modified differential equations, which are obtained as follows:

$$\begin{aligned}
&A_{11}\left(\sin\frac{n\pi y}{b}\right)e^{i\omega t}\frac{d^2U}{dX^2} - A_{66}\left(\sin\frac{n\pi y}{b}\right)e^{i\omega t}\left(\frac{n\pi y}{b}\right)^2 U\\
&-(A_{12}+A_{66})\left(\sin\frac{n\pi y}{b}\right)e^{i\omega t}\left(\frac{n\pi y}{b}\right)\frac{dV}{dX} = -I_0\omega^2\left(\sin\frac{n\pi y}{b}\right)e^{i\omega t}U
\end{aligned} \tag{10a}$$

$$\begin{aligned}
&(A_{66}+A_{12})\left(\cos\frac{n\pi y}{b}\right)e^{i\omega t}\left(\frac{n\pi}{b}\right)\frac{dU}{dX} + A_{66}\left(\cos\frac{n\pi y}{b}\right)e^{i\omega t}\frac{d^2V}{dX^2}\\
&-A_{22}\left(\cos\frac{n\pi y}{b}\right)e^{i\omega t}\left(\frac{n\pi}{b}\right)^2 V = -I_0\omega^2\left(\cos\frac{n\pi y}{b}\right)e^{i\omega t}V
\end{aligned} \tag{10b}$$

$$\begin{aligned}
&-H_{11}c_1^2\left(\sin\frac{n\pi y}{b}\right)e^{i\omega t}\frac{d^4W}{dx^4} + \left(2H_{12}c_1^2 + 4H_{66}c_1^2\right)\left(\sin\frac{n\pi y}{b}\right)e^{i\omega t}\left(\frac{n\pi}{b}\right)^2\frac{d^2W}{dx^2}\\
&-H_{22}c_1^2\left(\sin\frac{n\pi y}{b}\right)e^{i\omega t}\left(\frac{n\pi}{b}\right)^4 W + \left(A_{55}-2D_{55}c_2 + F_{55}c_2^2\right)\left(\sin\frac{n\pi y}{b}\right)e^{i\omega t}\frac{d^2W}{dx^2}\\
&-\left(A_{44}-2D_{44}c_2 + F_{44}c_2^2\right)\left(\sin\frac{n\pi y}{b}\right)e^{i\omega t}\left(\frac{n\pi}{b}\right)^2 W + \left(F_{11}c_1 - H_{11}c_1^2\right)\left(\sin\frac{n\pi y}{b}\right)e^{i\omega t}\frac{d^3\phi_x}{dx^3}\\
&-\left(2F_{66}c_1 - 2H_{66}c_1^2 + 2F_{12}c_1 - 2H_{12}c_1^2\right)\left(\sin\frac{n\pi y}{b}\right)e^{i\omega t}\left(\frac{n\pi}{b}\right)^2\frac{d\phi_x}{dx}\\
&+\left(A_{55}-2D_{55}c_2 + F_{55}c_2^2\right)\left(\sin\frac{n\pi y}{b}\right)e^{i\omega t}\frac{d\phi_x}{dx}\\
&-\left(F_{12}c_1 - H_{12}c_1^2 + 2F_{66}c_1 - 2H_{66}c_1^2\right)\left(\sin\frac{n\pi y}{b}\right)e^{i\omega t}\left(\frac{n\pi}{b}\right)\frac{d^2\phi_y}{dx^2}\\
&+\left(F_{22}c_1 - H_{22}c_1^2\right)\left(\sin\frac{n\pi y}{b}\right)e^{i\omega t}\left(\frac{n\pi}{b}\right)^3\phi_y - \left(A_{44}-2D_{44}c_2 + F_{44}c_2^2\right)\left(\sin\frac{n\pi y}{b}\right)e^{i\omega t}\left(\frac{n\pi}{b}\right)\phi_y\\
&= I_0\left(\sin\frac{n\pi y}{b}\right)e^{i\omega t}\left(-\omega^2\right)W - c_1^2 I_6\left(\left(\sin\frac{n\pi y}{b}\right)e^{i\omega t}\left(-\omega^2\right)\frac{d^2W}{dx^2} + \left(\sin\frac{n\pi y}{b}\right)\left(\frac{n\pi}{b}\right)^2 e^{i\omega t}\left(\omega^2\right)W\right)\\
&+c_1 J_4\left(\left(\sin\frac{n\pi y}{b}\right)e^{i\omega t}\left(-\omega^2\right)\frac{d\phi_x}{dx} + \left(\sin\frac{n\pi y}{b}\right)\left(\frac{n\pi}{b}\right)e^{i\omega t}\left(\omega^2\right)\phi_y\right)
\end{aligned} \tag{10c}$$

$$\left(H_{11}c_1^2 - F_{11}c_1\right)\left(\sin\frac{n\pi y}{b}\right)e^{i\omega t}\frac{d^3W}{dx^3} - \left(H_{12}c_1^2 - F_{12}c_1 + 2H_{66}c_1^2 - 2F_{66}c_1\right)\left(\sin\frac{n\pi y}{b}\right)e^{i\omega t}\left(\frac{n\pi}{b}\right)^2\frac{dW}{dx}$$
$$-\left(A_{55} - 2D_{55}c_2 + F_{55}c_2^2\right)\left(\sin\frac{n\pi y}{b}\right)e^{i\omega t}\frac{dW}{dx}$$
$$+\left(D_{11} - 2F_{11}c_1 + H_{11}c_1^2\right)\left(\sin\frac{n\pi y}{b}\right)e^{i\omega t}\frac{d^2\phi_x}{dx^2}$$
$$-\left(D_{66} - 2F_{66}c_1 + H_{66}c_1^2\right)\left(\sin\frac{n\pi y}{b}\right)e^{i\omega t}\left(\frac{n\pi}{b}\right)^2\phi_x \qquad (10d)$$
$$-\left(A_{55} - 2D_{55}c_2 + F_{55}c_2^2\right)\left(\sin\frac{n\pi y}{b}\right)e^{i\omega t}\phi_x$$
$$-\left(D_{12} - 2F_{12}c_1 + H_{12}c_1^2 + D_{66} - 2F_{66}c_1 + H_{66}c_1^2\right)\left(\sin\frac{n\pi y}{b}\right)e^{i\omega t}\left(\frac{n\pi}{b}\right)\frac{d\phi_y}{dx}$$
$$= K_2\left(\sin\frac{n\pi y}{b}\right)e^{i\omega t}\left(-\omega^2\right)\phi_x - c_1 J_4\left(\sin\frac{n\pi y}{b}\right)e^{i\omega t}\left(-\omega^2\right)\frac{dW}{dx}$$

$$\left(2H_{66}c_1^2 - 2F_{66}c_1 + H_{12}c_1^2 - F_{12}c_1\right)\left(\cos\frac{n\pi y}{b}\right)e^{i\omega t}\left(\frac{n\pi}{b}\right)\frac{d^2W}{dx^2} - \left(H_{22}c_1^2 - F_{22}c_1\right)\left(\cos\frac{n\pi y}{b}\right)e^{i\omega t}\left(\frac{n\pi}{b}\right)^3 W$$
$$-\left(A_{44} - 2D_{44}c_2 + F_{44}c_2^2\right)\left(\cos\frac{n\pi y}{b}\right)e^{i\omega t}\left(\frac{n\pi}{b}\right)W$$
$$+\left(D_{66} - 2F_{66}c_1 + H_{66}c_1^2 + D_{12} - 2F_{12}c_1 + H_{12}c_1^2\right)\left(\cos\frac{n\pi y}{b}\right)e^{i\omega t}\left(\frac{n\pi}{b}\right)\frac{d\phi_x}{dx} \qquad (10e)$$
$$+\left(D_{66} - 2F_{66}c_1 + H_{66}c_1^2\right)\left(\cos\frac{n\pi y}{b}\right)e^{i\omega t}\frac{d^2\phi_y}{dx^2}$$
$$-\left(D_{22} - 2F_{22}c_1 + H_{22}c_1^2\right)\left(\cos\frac{n\pi y}{b}\right)e^{i\omega t}\left(\frac{n\pi}{b}\right)^2\phi_y - \left(A_{44} - 2D_{44}c_2 + F_{44}c_2^2\right)\left(\cos\frac{n\pi y}{b}\right)e^{i\omega t}\phi_y$$
$$= K_2\left(\cos\frac{n\pi y}{b}\right)e^{i\omega t}\left(-\omega^2\right)\phi_y - c_1 J_4\left(\cos\frac{n\pi y}{b}\right)e^{i\omega t}\left(-\omega^2\right)W$$

where

$$\lambda^2 = \frac{I_0\omega^2 a^2}{A_{11}}$$

Method of Solution

Equation (10) contains derivatives of supplanting and turning functions. Spline approximation is used to approximate these functions, with X having a range between [0, 1]. The purpose of using splines for approximation is for their high precision and rapid rate of convergence (Schoenberg and Witney [33]).

The spline approximation defines the supplanting $U(X)$, $V(X)$, $W(X)$, and the turning functions $\Phi_X(X)$, $\Phi_Y(X)$ as follows:

$$U(X) = \sum_{i=0}^{4} a_i X^i + \sum_{j=0}^{N-1} b_j (X - X_j)^5 H(X - X_j)$$

$$V(X) = \sum_{i=0}^{2} c_i X^i + \sum_{j=0}^{N-1} d_j (X - X_j)^3 H(X - X_j)$$

$$W(X) = \sum_{i=0}^{4} e_i X^i + \sum_{j=0}^{N-1} f_j (X - X_j)^5 H(X - X_j) \qquad (11)$$

$$\Phi_X(X) = \sum_{i=0}^{4} g_i X^i + \sum_{j=0}^{N-1} g_j (X - X_j)^5 H(X - X_j)$$

$$\Phi_Y(X) = \sum_{i=0}^{2} l_i X^i + \sum_{j=0}^{N-1} q_j (X - X_j)^3 H(X - X_j)$$

Here, $H(X - X_j)$ is the Heaviside step function and the range of X, which is [0, 1], and is divided into the number of intervals (N). The knots of the splines are selected as the points $X = X_s = \frac{s}{N}$, ($s = 0, 1, 2, \ldots, N$). Therefore, Equation (10) is satisfied by the splines. The subsequent set of equations contain $(5N + 5)$, a homogeneous system of equations in the $(5N + 21)$ spline coefficients. Considering simply supported boundary conditions, three spline coefficients become zero. In return, this gives 13 more equations,

thus making a total of $(5N + 18)$ equations and the same number of unknowns, which are represented by the following form:

$$[\,K\,]\,\{\,j\,\} \ = \ \lambda^2\,[\,L\,]\,\{\,j\,\} \tag{12}$$

The global eigenvalue problem is obtained with the eigenparameter λ and the eigen-vector $\{\,j\,\}$. Here, in Equation (12), $[\,K\,]$ and $[\,L\,]$ are square matrices and $\{\,j\,\}$ is a column matrix consisting of spline coefficients.

3. Results and Discussion

The research shows that the obtained results are in good agreement with the existing literature. The parametric effects of plates' aspect ratio, side-to-tickness ratio, assembling sequence, number of composite layers, and alignment of each layer on the frequency of the plate are studied. The results show that the aspect ratio and the side-to-tickness ratio have a significant effect on the frequency of the plate. The number of composite layers and alignment of each layer also affects the frequency of the plate, but to a lesser extent. For all numerical computations in this section, unless otherwise stated, the material considered is Kevlar-49/epoxy. Three-, five-, and six-layered plates having symmetric orientations are considered.

Kevler-49 epoxy material properties
$\rho = 1440$, $E_T = 5.52$, $E_L = 86.19$, $\mu_{LT} = 0.34$, $G_{LT} = 2.07$, $G_{LZ} = 2.07$, $G_{TZ} = 1.72$.

3.1. Convergence Study

The convergence study validates the convergence of the spline method for symmetric angle ply plates, as shown in Table 1. The number of subintervals N of the range $X \in [0, 1]$. The value of N started from 4 and finally it is fixed for $N = 12$ since for the next value of N, the percent changes in the values of λ are very low, the maximum being 2%.

Table 1. Convergence for the frequency parameters of four layered anti-symmetric plates under C-C boundary conditions.

N	λ_1	% Change	λ_2	% Change	λ_3	% Change
4	0.547064	-	1.260471	-	2.0610	-
6	0.511985	-6.41222	1.12029	-11.12131	1.894131	-8.09650
8	0.499459	-2.46555	1.069711	-4.51481	1.761941	-6.97892
10	0.493624	-1.16826	1.046288	-2.18965	1.700053	-3.51248
12	0.490446	-0.64380	1.033585	-1.21410	1.666535	-1.97158

3.2. Validation

The comparative study was carried out to validate the present results in Table 2. The reduced case of the present study was compared by Shi et al. [34] and Xiang et al. [35]. The present results show a close agreement with the available results by Shi et al. [34] and Xiang et al. [35].

Table 2. Comparison of non-dimensional frequencies of square clamped supported plate with $a/h = 10$, 20, 100. Results are compared with Shi et al. [34] and Xiang et al. [35].

a/h	Method	Mode 1	2	3
	Shi et al. [34]	17.433	22.506	30.905
10	Xiang et al. [35]	17.225	22.261	30.631
	Present	17.333	22.576	30.981
	Shi et al. [34]	23.979	30.407	41.937
20	Xiang et al. [35]	23.745	30.041	41.295
	Present	23.854	30.342	41.821

Table 2. *Cont.*

a/h	Method	Mode 1	2	3
	Shi et al. [34]	28.946	36.772	50.721
100	Xiang et al. [35]	28.572	36.184	49.791
	Present	28.734	36.634	50.612

Discussion: The research provides a numerical analysis solution for symmetric angle ply plates using HSDT. The results obtained from the research can be used to study the frequency response of the plate and the parametric effects of various plate configurations. The research highlights the importance of considering the aspect ratio and the side-to-thickness ratio when designing symmetric angle ply plates.

3.3. Frequency Parameter Variation under Different Ply Angles of Symmetric Plates

Table 3 shows that the value of the frequency parameter increases with the increase in ply angle. It also depicts that as the number of layers of composite plates decreases the frequency, the parameter value also decreases. It is known that the stiffness decrease or increase according to the frequency parameter value decreases or increases. In this study, as the number of layers of plates decreases, the frequency parameter value also decreases, which shows that its stiffness decreases and flexibility increases.

Table 3. The fundamental frequency of different layered plates by varying ply angles.

θ	6-Layered λ	5-Layered λ	3-Layered λ
$10°$	0.262205	0.249637	0.246888
$20°$	0.276866	0.269521	0.259949
$30°$	0.332592	0.307604	0.309678
$40°$	0.417498	0.404969	0.385188
$50°$	0.53254	0.515285	0.497382
$60°$	0.696845	0.673437	0.643287
$70°$	0.899267	0.869292	0.83807

3.4. Frequency Parameter Variation under the Effect of the Aspect Ratio, Side-to-Thickness Ratio, and Ply Angle of Symmetric Plates

Figures 2–4 show the effect of the aspect ratio on the frequency parameter of symmetric angle ply plates of 6-layered plates under simply supported boundary conditions. Different ply angle orientations were used. It shows that as the aspect ratio increases, the frequency increases gradually. This shows that the rigidity of the structure increases with the increase in frequency values and its flexibility decreases.

Figures 5–7 demonstrate the variation of the side-to-thickness ratio and frequency parameter of plates of different symmetric ply orientations. The curvature of the graph curve elucidates that as the side-to-thickness ratio value increases, the frequency parameter value decreases.

Figures 8–10 explicate the effect of ply angle on the frequency parameter value of 6-layered composite plates. They show that as the ply angle increases, the frequency value also increases.
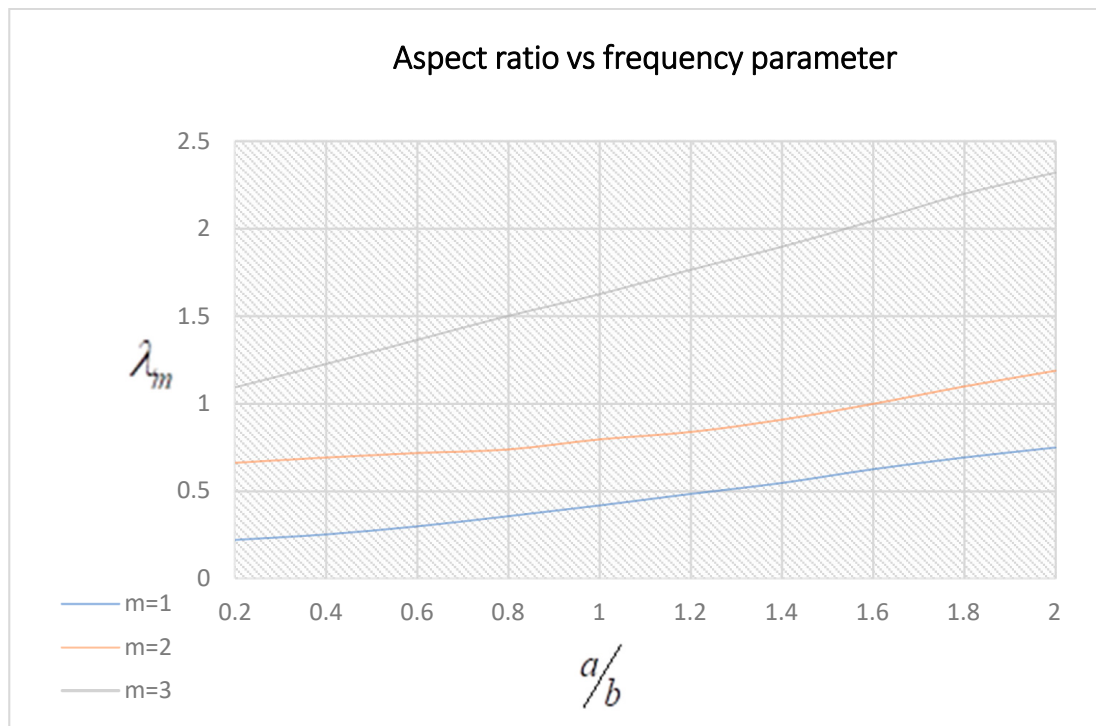
Figure 2. Variation of the aspect ratio vs. frequency parameter of 6-layered plates $45^{\circ}/30^{\circ}/0^{\circ}/0^{\circ}/30^{\circ}/45^{\circ}$.
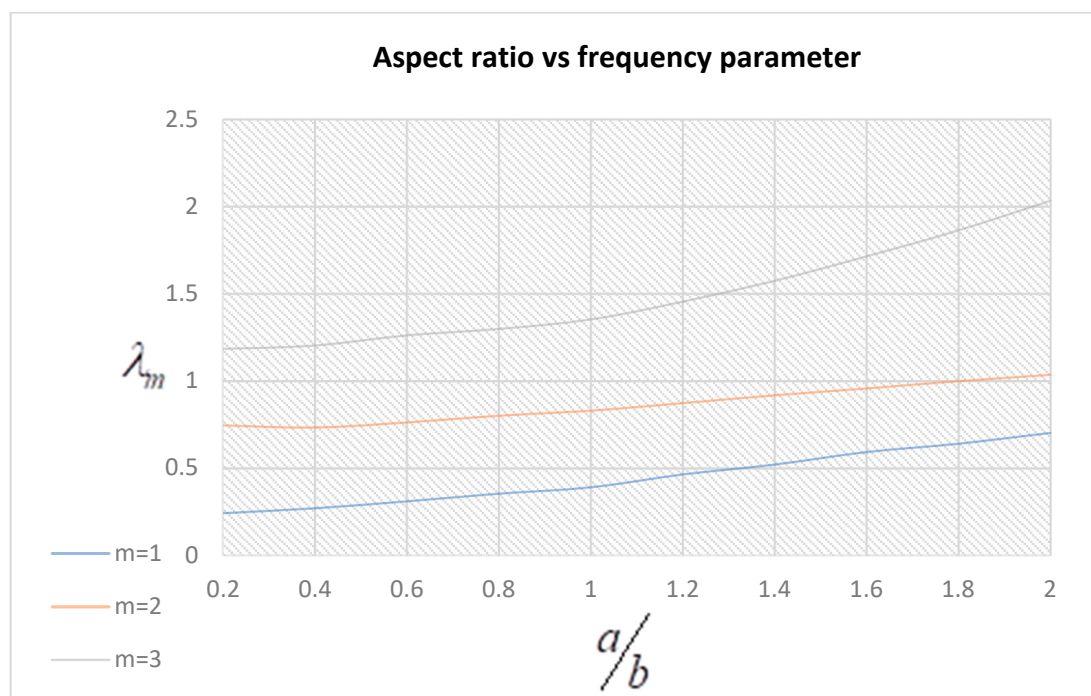

Figure 3. Variation of the aspect ratio vs. frequency parameter of 6-layered plates $30^{\circ}/45^{\circ}/0^{\circ}/0^{\circ}/45^{\circ}/30^{\circ}$.
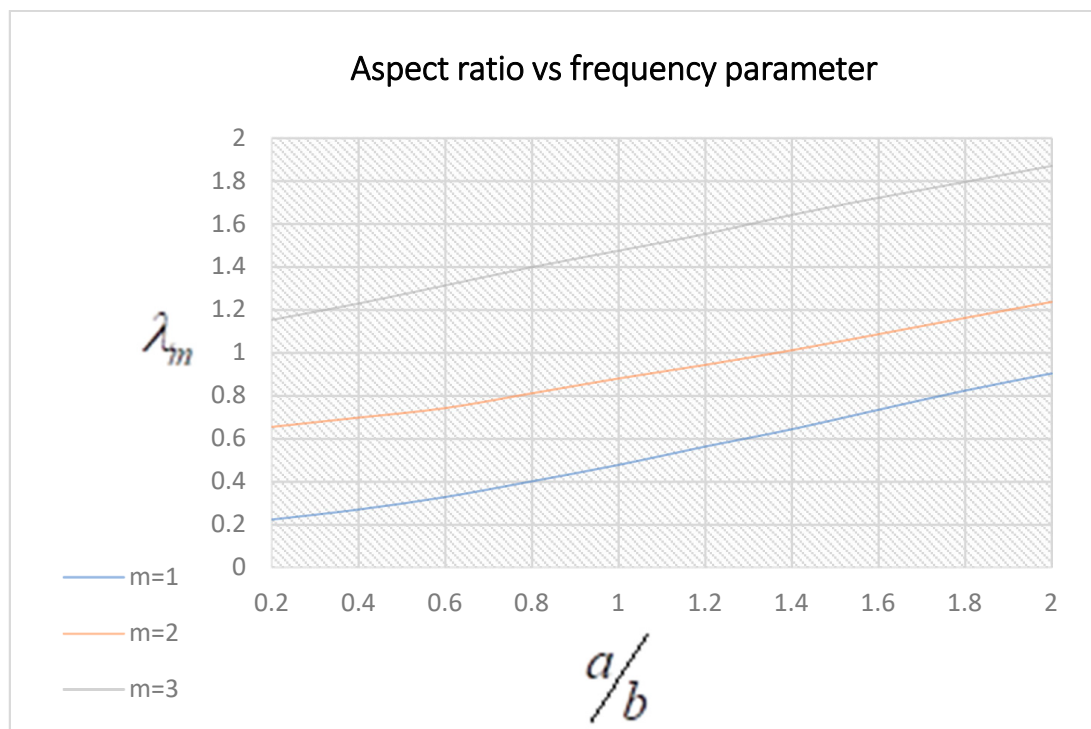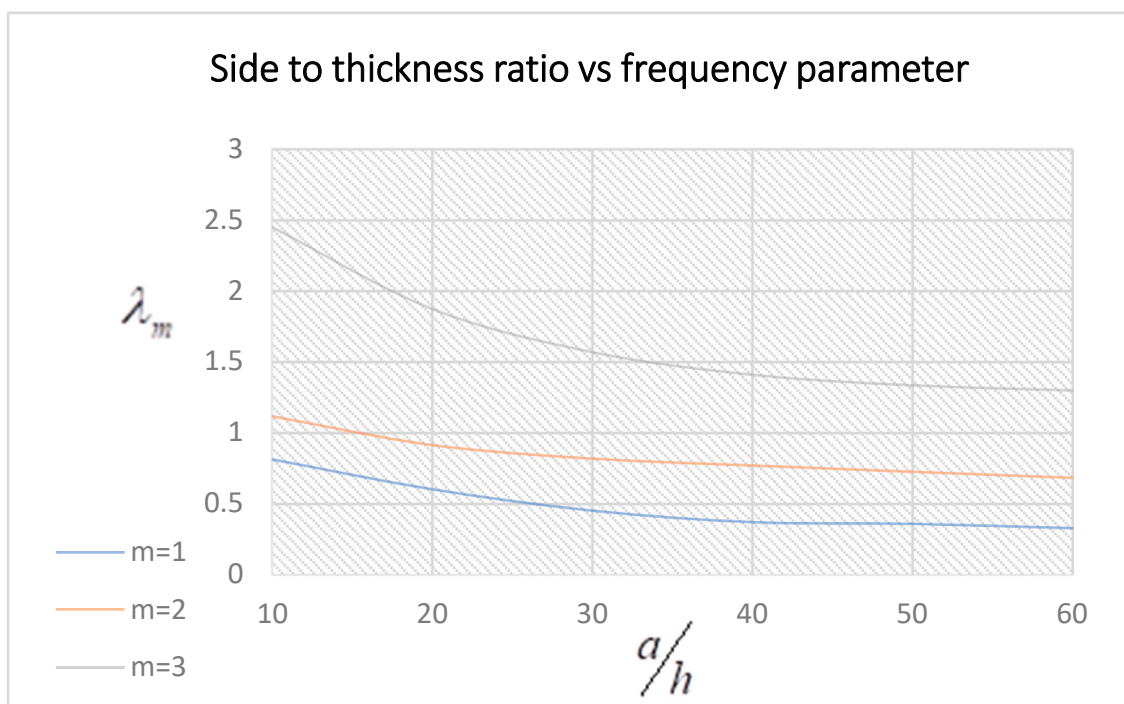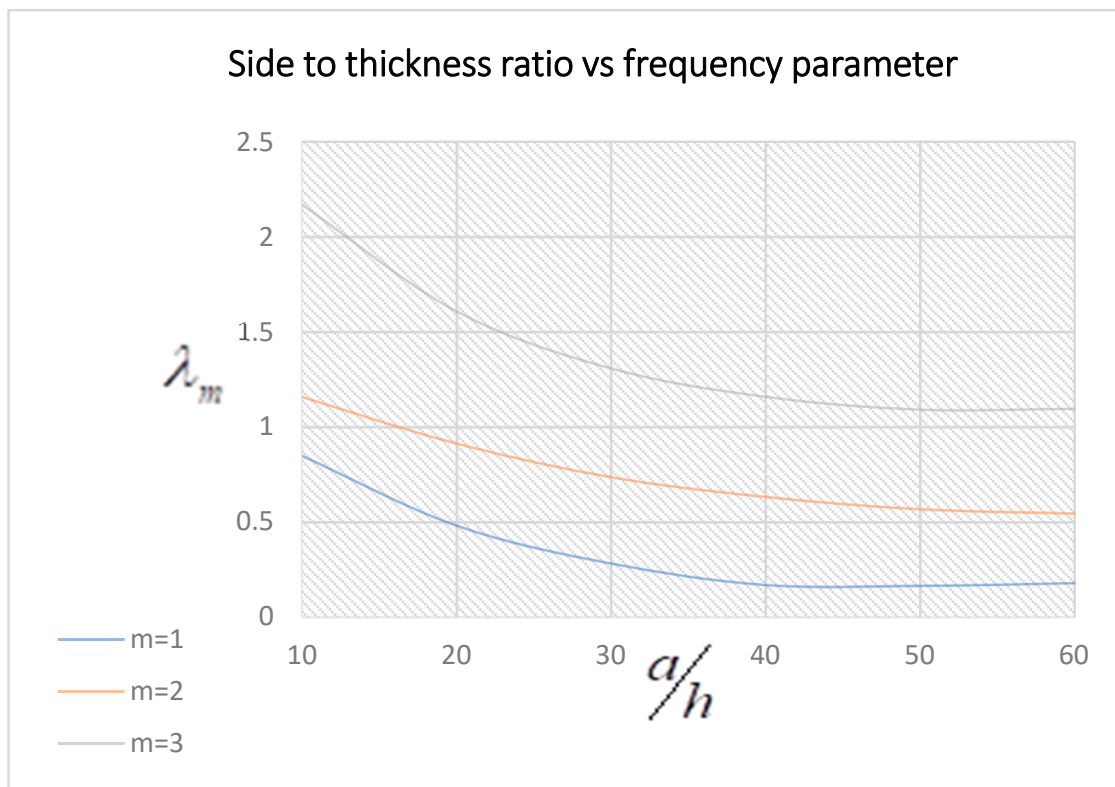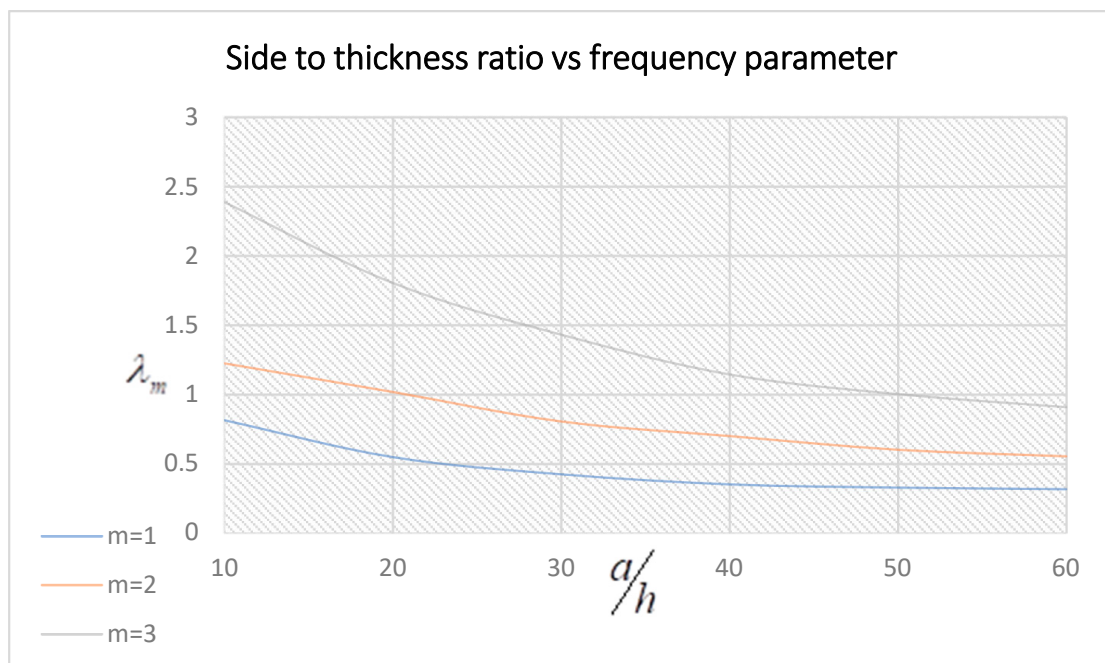
Figure 4. Variation of the aspect ratio vs. frequency parameter of 6-layered plates $45°/60°/0°/0°/60°/45°$.

Figure 5. Variation of the side-to-thickness ratio vs. frequency parameter of 5-layered plates $45°/60°/0°/60°/45°$.

Side to thickness ratio vs frequency parameter

Figure 6. Variation of side-to-thickness ratio vs. frequency parameter of 6-layered plates $30°/45°/0°/0°/45°/30°$.

Side to thickness ratio vs frequency parameter

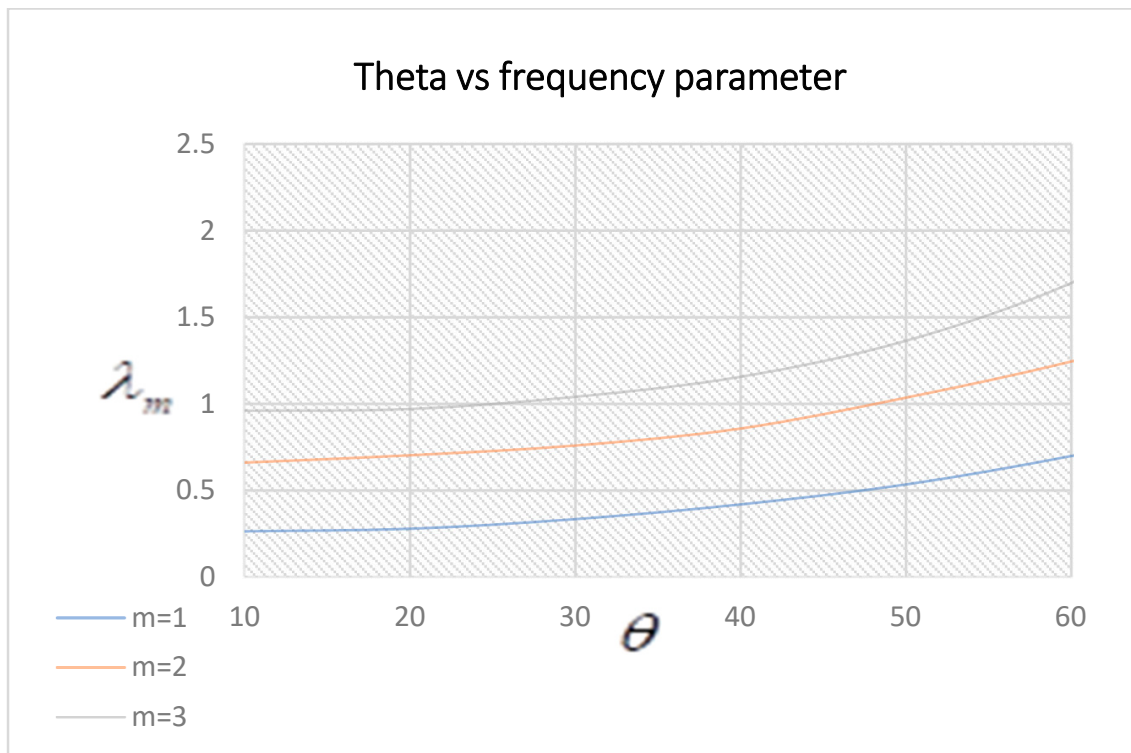**Figure 7.** Variation of side-to-thickness ratio vs. frequency parameter of 6-layered plates $60°/45°/0°/0°/45°/60°$.

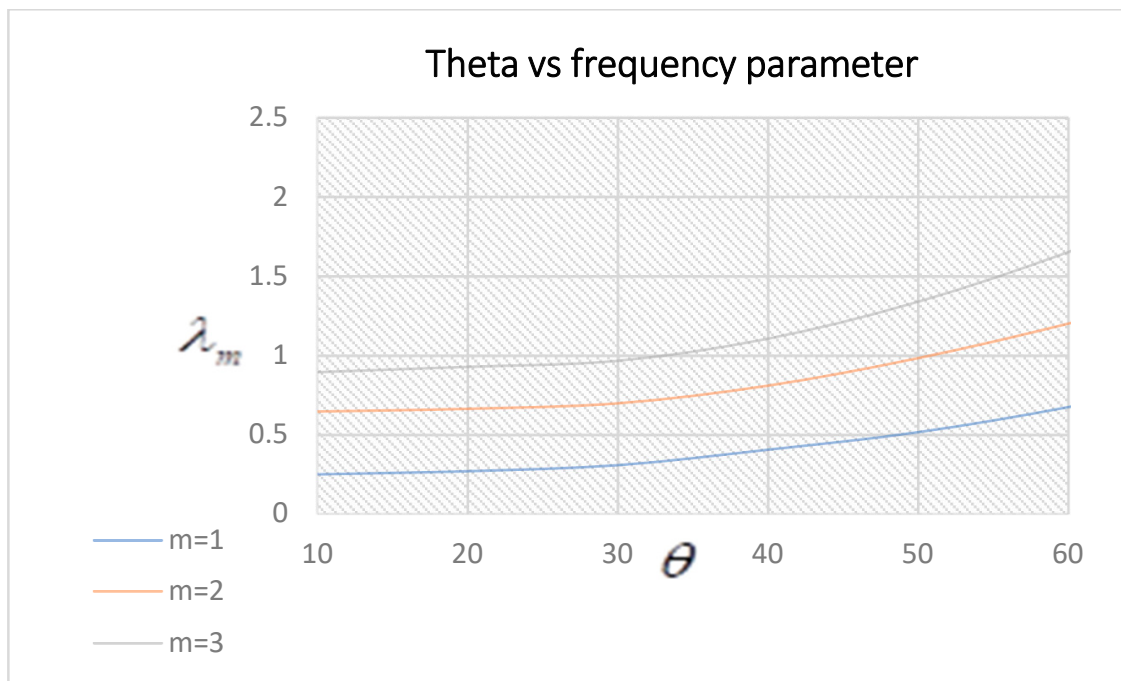**Figure 8.** Variation of the theta vs. frequency parameter of 6-layered plates.

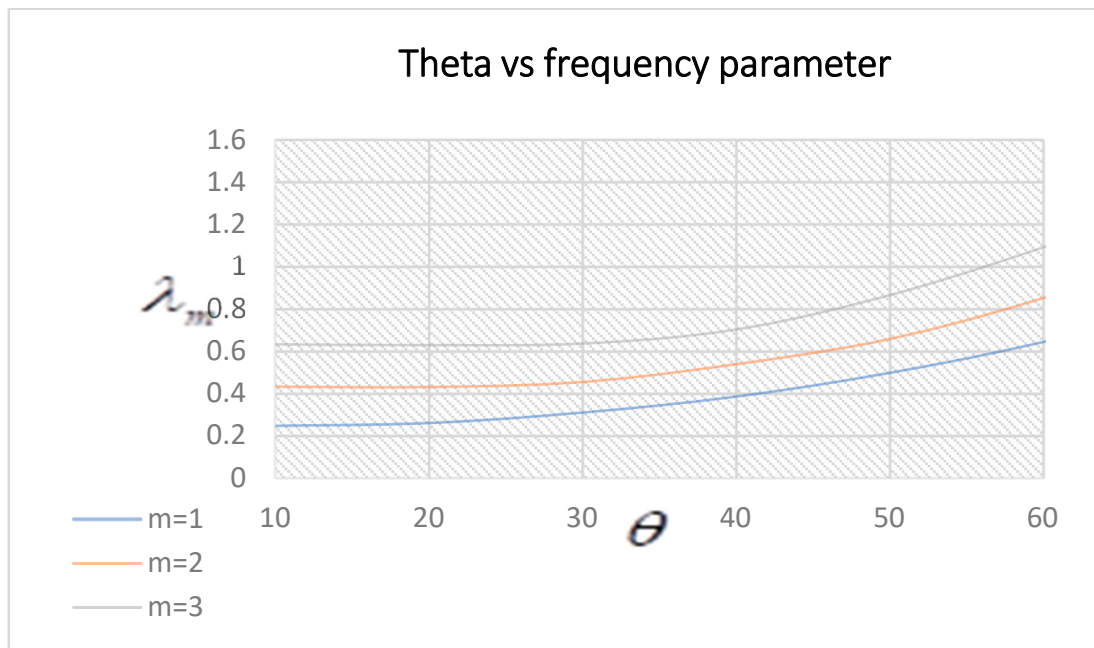**Figure 9.** Variation of the theta vs. frequency parameter of 5-layered plates.

Figure 10. Variation of the theta vs. frequency parameter of 3-layered plates.

4. Conclusions

The research provides a numerical analysis solution for symmetric angle ply plates using HSDT under simply supported support conditions. The results obtained from the research can be used to study the frequency response of the plate and the parametric effects of various plate configurations. The research highlights the importance of considering the aspect ratio and the side-to-thickness ratio when designing symmetric angle ply plates. The effect of the aspect ratio on the frequency parameter is that with the increase in the aspect ratio, the frequency increases gradually. Moreover, as the side-to-thickness ratio increases, the frequency parameter value decreases. In addition to this, as the ply angle increases, the frequency value also increases. It is evident from these results that as the number of layers of plates decreases, the frequency parameter value also decreases, which shows that as the stiffness of a structure decreases, the flexibility increases. However, with the increase in the aspect ratio and the side-to-thickness ratio, the frequency increases, which shows that as the rigidity of a structure increases, the flexibility decreases.

The obtained results are validated by existing literature.

Data Availability Statement: The data supporting the results of this study are included in the manuscript.

Conflicts of Interest: The author declares that they have no conflicts of interest regarding the publication of this paper.

Nomenclature

A_{ij}	Elastic coefficients representing the extensional rigidity
B_{ij}	Elastic coefficients representing the bending–stretching coupling rigidity
D_{ij}	Elastic coefficients representing the bending rigidity

$\left.\begin{array}{l}G_{LT}^{(k)}\\G_{LZ}^{(k)}\\G_{TZ}^{(k)}\end{array}\right\}$	Shear modulus in the respective directions of the k-th layer
H	Side-to-thickness ratio
$H(X-X_j)$	The Heaviside step function
I_1	Normal inertia coefficient
I_3	Rotary inertia coefficients
L	Length parameter
$\left.\begin{array}{l}M_x\\M_y\\M_{xy}\end{array}\right\}$	Moment resultants in the respective directions of the plate
$\left.\begin{array}{l}N_x\\N_y\\N_{xy}\end{array}\right\}$	Stress results in the respective direction of the plate
N	Number of intervals of spline interpolation
$Q_{ij}^{(k)}$	Elements of the stiffness matrix for the material of the k-th layer
$\overline{Q}_{ij}^{(k)}$	Elements of the transformed stiffness matrix for the material of the k-th layer
$\left.\begin{array}{l}Q_{xz}\\Q_{yz}\end{array}\right\}$	Transverse shear resultants in the respective directions of the plate
$U,\ V,\ W$	Displacement functions in the x, y, and z directions of the plate
X	Nondimensionalized distance co-ordinate of the plate
X_s	The equally spaced knots of spline interpolation
a, b	Length and width of the plates
$\left.\begin{array}{l}a_i\\c_i\\e_i\\g_i\\l_i\end{array}\right\},\ \left.\begin{array}{l}b_j\\d_j\\f_j\\p_j\\q_j\end{array}\right\}$	Spline coefficients
h	The total thickness of the plate
h_k	The thickness of the k-th layer of the plate
i, j, k	Summation or general indices
$u,\ v,\ w$	x, y, and z displacements of the plate
$u_0,\ v_0$	The in-plane displacements of the reference surface
x	Length coordinate of the plate
y	Width coordinate of the plate
z	Normal coordinate of any point on the plate
z_k	Distance of the top of the k-th layer from the reference surface
β	Product of $n\pi(a/b)$ of the plate
δ_k	The relative layer thickness of the k-th layer
$\left.\begin{array}{l}\varepsilon_x\\\varepsilon_y\end{array}\right\}$	Normal strain in the respective directions
$\left.\begin{array}{l}\gamma_{xy}\\\gamma_{xz}\\\gamma_{yz}\end{array}\right\}$	Shear strain in the respective directions of the plate
$\left.\begin{array}{l}\kappa_x\\\kappa_y\\\kappa_{xy}\end{array}\right\}$	The changes in the curvature of the reference surface during deformation in the respective directions of the plate Non-dimensional frequency parameter
λ	
$\psi_x,\ \psi_y$	Shear rotations of any point on the middle surface of the plate
$\Psi_x,\ \Psi_y$	Shear rotational functions of the plate
$\overline{\Psi}_X,\ \overline{\Psi}_Y$	Non-dimensionalized shear rotations of the plate
ρ	The mass density of the material of the plate or shell
$\left.\begin{array}{l}\sigma_x\\\sigma_y\end{array}\right\}$	Normal stress in the respective directions of the plate
$\left.\begin{array}{l}\tau_{xy}\\\tau_{yz}\\\tau_{xz}\end{array}\right\}$	Shear stress at a point on the reference surface of the plate
θ	Ply orientation angle

Appendix A

Appendix A.1. Components of the Stiffness Matrix for the of k-th Layer of Plate Material

$$Q_{11}^{(k)} = \frac{E_x^{(k)}}{1 - v_{xy}^{(k)} v_{yx}^{(k)}}, Q_{12}^{(k)} = \frac{v_{xy}^{(k)} E_y^{(k)}}{1 - v_{xy}^{(k)} v_{yx}^{(k)}} = \frac{v_{yx}^{(k)} E_x^{(k)}}{1 - v_{xy}^{(k)} v_{yx}^{(k)}}, Q_{22}^{(k)} = \frac{E_y^{(k)}}{1 - v_{xy}^{(k)} v_{yx}^{(k)}},$$

$$Q_{66}^{(k)} = G_{xy}^{(k)}, Q_{44}^{(k)} = G_{yz}^{(k)}, Q_{55}^{(k)} = G_{xz}^{(k)} \tag{A1}$$

Appendix A.2. Components of the Transformed Stiffness Matrix for the k-th Layer Material

$$\overline{Q}_{11}^{(k)} = Q_{11}^{(k)} \cos^4\theta + Q_{22}^{(k)} \sin^4\theta + 2\left(Q_{12}^{(k)} + 2Q_{66}^{(k)}\right) \sin^2\theta \cos^2\theta \tag{A2}$$

$$\overline{Q}_{22}^{(k)} = Q_{11}^{(k)} \sin^4\theta + Q_{22}^{(k)} \cos^4\theta + 2\left(Q_{12}^{(k)} + 2Q_{66}^{(k)}\right) \sin^2\theta \cos^2\theta \tag{A3}$$

$$\overline{Q}_{12}^{(k)} = \left(Q_{11}^{(k)} + Q_{22}^{(k)} - Q_{66}^{(k)}\right) \sin^2\theta \cos^2\theta + Q_{12}^{(k)} \left(\cos^4\theta + \sin^4\theta\right) \tag{A4}$$

$$\overline{Q}_{16}^{(k)} = \left(Q_{11}^{(k)} - Q_{12}^{(k)} - 2Q_{66}^{(k)}\right) \cos^3\theta \sin\theta - \left(Q_{22}^{(k)} - Q_{12}^{(k)} - 2Q_{66}^{(k)}\right) \sin^3\theta \cos\theta \tag{A5}$$

$$\overline{Q}_{26}^{(k)} = \left(Q_{11}^{(k)} - Q_{12}^{(k)} - 2Q_{66}^{(k)}\right) \cos\theta \sin^3\theta - \left(Q_{22}^{(k)} - Q_{12}^{(k)} - 2Q_{66}^{(k)}\right) \sin\theta \cos^3\theta \tag{A6}$$

$$\overline{Q}_{66}^{(k)} = \left(Q_{11}^{(k)} + Q_{22}^{(k)} - 2Q_{12}^{(k)} - 2Q_{66}^{(k)}\right) \cos^2\theta \sin^2\theta + Q_{66}^{(k)} \left(\sin^4\theta + \cos^4\theta\right) \tag{A7}$$

$$\overline{Q}_{44}^{(k)} = Q_{55}^{(k)} \sin^2\theta + Q_{44}^{(k)} \cos^2\theta \tag{A8}$$

$$\overline{Q}_{55}^{(k)} = Q_{55}^{(k)} \cos^2\theta + Q_{44}^{(k)} \sin^2\theta \tag{A9}$$

$$\overline{Q}_{45}^{(k)} = \left(Q_{55}^{(k)} - Q_{44}^{(k)}\right) \cos\theta \sin\theta \tag{A10}$$

where,

$$\left[\overline{Q}^{(k)}\right] = [T]\left[Q^{(k)}\right][T]^{-1}$$

$$[T] = \begin{bmatrix} \cos^2\theta & \sin^2\theta & 0 & 0 & -2\sin\theta\cos\theta \\ \sin^2\theta & \cos^2\theta & 0 & 0 & 2\sin\theta\cos\theta \\ 0 & 0 & \cos\theta & \sin\theta & 0 \\ 0 & 0 & -\sin\theta & \cos\theta & 0 \\ \sin\theta\cos\theta & -\sin\theta\cos\theta & 0 & 0 & \cos^2\theta - \sin^2\theta \end{bmatrix}$$

References

1. Vinson, J.R. Sandwich Structures. *Appl. Mech. Rev.* **2001**, *54*, 201–214. [CrossRef]
2. Noor, A.K.; Burton, W.S.; Bert, C.W. Computational models for sandwich panels and shells. *Appl. Mech. Rev.* **1996**, *49*, 155–199. [CrossRef]
3. Yang, P.C.; Nooris, C.H.; Stavsky, Y. Elastic wave propogation in heterogeneous plates. *Int. J. Solids Struct.* **1966**, *2*, 665–684. [CrossRef]
4. Reddy, J.N. *Theory and Analysis of Elastic Plates and Shells*; CRC Press: Boca Raton, FL, USA, 2006.
5. Ghiamy, A.; Amoushahi, H. Dynamic stability of different kinds of sandwich plates using third order shear deformation theory. *Thin-Walled Struct.* **2022**, *172*, 108822. [CrossRef]
6. Parida, S.P.; Jena, P.C. Free and forced vibration analysis of flyash/graphene filled laminated composite plates using higher order shear deformation theory. *Proc. Inst. Mech. Eng. Part C J. Mech. Eng. Sci.* **2022**, *236*, 4648–4659. [CrossRef]
7. Zhao, Y.; Qin, B.; Wang, Q.; Liang, X. A unified Jacobi–Ritz approach for the FGP annular plate with arbitrary boundary conditions based on a higher-order shear deformation theory. *J. Vib. Control* **2022**. [CrossRef]
8. Tian, Y.; Li, Q.; Wu, D.; Chen, X.; Gao, W. Nonlinear dynamic stability analysis of clamped and simply supported organic solar cells via the third-order shear deformation plate theory. *Eng. Struct.* **2022**, *252*, 113616. [CrossRef]
9. Belkhodja, Y.; Ouinas, D.; Fekirini, H.; Olay, J.A.; Achour, B.; Touahmia, M.; Boukendakdji, M. A new hybrid HSDT for bending, free vibration, and buckling analysis of FGM plates (2D & quasi-3D). *Smart Struct. Syst.* **2022**, *29*, 395–420.

10. Eskandari Shahraki, M.; Shariati, M.; Asiaban, N.; Davar, A.; Heydari Beni, M.; Eskandari Jam, J. Assessment of Third-order Shear Deformation Graphene Nanoplate Response under Static Loading Using Modified Couple Stress Theory. *J. Mod. Process. Manuf. Prod.* **2022**, *11*, 41–57.

11. Shi, P.; Dong, C. A refined hyperbolic shear deformation theory for nonlinear bending and vibration isogeometric analysis of laminated composite plates. *Thin-Walled Struct.* **2022**, *174*, 109031. [CrossRef]

12. Javani, M.; Kiani, Y.; Eslami, M.R. On the free vibrations of FG-GPLRC folded plates using GDQE procedure. *Compos. Struct.* **2022**, *286*, 115273. [CrossRef]

13. Sayyad, A.S.; Avhad, P.V. A new higher order shear and normal deformation theory for the free vibration analysis of sandwich curved beams. *Compos. Struct.* **2022**, *280*, 114948. [CrossRef]

14. Ellali, M.; Bouazza, M.; Amara, K. Thermal buckling of a sandwich beam attached with piezoelectric layers via the shear deformation theory. *Arch. Appl. Mech.* **2022**, *92*, 657–665. [CrossRef]

15. Nguyen, N.D.; Nguyen, T.N.; Nguyen, T.K.; Vo, T.P. A new two-variable shear deformation theory for bending, free vibration and buckling analysis of functionally graded porous beams. *Compos. Struct.* **2022**, *282*, 115095. [CrossRef]

16. Peng, L.X.; Chen, S.Y.; Wei, D.Y.; Chen, W.; Zhang, Y.S. Static and free vibration analysis of stiffened FGM plate on elastic foundation based on physical neutral surface and MK method. *Compos. Struct.* **2022**, *290*, 115482. [CrossRef]

17. Pham, Q.H.; Tran, T.T.; Tran, V.K.; Nguyen, P.C.; Nguyen-Thoi, T. Free vibration of functionally graded porous non-uniform thickness annular-nanoplates resting on elastic foundation using ES-MITC3 element. *Alex. Eng. J.* **2022**, *61*, 1788–1802. [CrossRef]

18. Hung, P.T.; Phung-Van, P.; Thai, C.H. A refined isogeometric plate analysis of porous metal foam microplates using modified strain gradient theory. *Compos. Struct.* **2022**, *289*, 115467. [CrossRef]

19. Sharma, N.; Swain, P.K.; Maiti, D.K.; Singh, B.N. Static and free vibration analyses and dynamic control of smart variable stiffness laminated composite plate with delamination. *Compos. Struct.* **2022**, *280*, 114793. [CrossRef]

20. Cho, J.R. Nonlinear free vibration of functionally graded CNT-reinforced composite plates. *Compos. Struct.* **2022**, *281*, 115101. [CrossRef]

21. Zang, Q.; Liu, J.; Ye, W.; Yang, F.; Hao, C.; Lin, G. Static and free vibration analyses of functionally graded plates based on an isogeometric scaled boundary finite element method. *Compos. Struct.* **2022**, *288*, 115398. [CrossRef]

22. Ghosh, S.; Haldar, S. Free Vibration analysis of isotropic and laminated composite plate on elastic point supports using finite element method. In *Recent Advances in Computational and Experimental Mechanics*; Springer: Singapore, 2022; Volume II, pp. 371–384.

23. Milazzo, A. Free vibrations analysis of cracked variable stiffness composite plates by the extended Ritz method. *Mech. Adv. Mater. Struct.* **2022**. [CrossRef]

24. Saiah, B.; Bachene, M.; Guemana, M.; Chiker, Y.; Attaf, B. On the free vibration behavior of nanocomposite laminated plates contained piece-wise functionally graded graphene-reinforced composite plies. *Eng. Struct.* **2022**, *253*, 113784. [CrossRef]

25. Singh, A.; Karathanasopoulos, N. Three-dimensional analytical elasticity solution for the mechanical analysis of arbitrarily-supported, cross and angle-ply composite plates under patch loads. *Compos. Struct.* **2023**, *310*, 116752. [CrossRef]

26. Belardi, V.G.; Fanelli, P.; Vivio, F. Application of the Ritz method for the bending and stress analysis of thin rectilinear orthotropic composite sector plates. *Thin-Walled Struct.* **2023**, *183*, 110374. [CrossRef]

27. Zhong, R.; Hu, S.; Liu, X.; Qin, B.; Wang, Q.; Shuai, C. Vibro-acoustic analysis of a circumferentially coupled composite laminated annular plate backed by double cylindrical acoustic cavities. *Ocean. Eng.* **2022**, *257*, 111584. [CrossRef]

28. Wang, H.; Zhao, X.; Gao, H.; Yuan, T.; Liu, X.; Zhang, W. Effects of alkali-treated plant wastewater on the properties and microstructures of alkali-activated composites. *Ceram. Int.* **2023**, *49*, 8583–8597. [CrossRef]

29. Zhang, Y.; Liu, G.; Ye, J.; Lin, Y. Crushing and parametric studies of polygonal substructures based hierarchical cellular honeycombs with non-uniform wall thickness. *Compos. Struct.* **2022**, *299*, 116087. [CrossRef]

30. Zhang, H.; Ouyang, Z.; Li, L.; Ma, W.; Liu, Y.; Chen, F.; Xiao, X. Numerical study on welding residual stress distribution of corrugated steel webs. *Metals* **2022**, *12*, 1831. [CrossRef]

31. Peng, J.; Xu, C.; Dai, B.; Sun, L.; Feng, J.; Huang, Q. Numerical Investigation of Brittleness Effect on Strength and Microcracking Behavior of Crystalline Rock. *Int. J. Geomech.* **2022**, *22*, 04022178. [CrossRef]

32. Reddy, J.N. *Mechanis of Laminated Composite Plates and Shells*; CRC Press: Boca Raton, FL, USA, 2003.

33. Schoenberg, I.J.; Whitney, A. On Pólya frequence functions. III. The positivity of translation determinants with an application to the interpolation problem by spline curves. *Trans. Am. Math. Soc.* **1953**, *74*, 246–259. [CrossRef]

34. Shi, J.W.; Nakatani, A.; Kitagawa, H. Vibration analysis of fully clamped arbitrarily laminated plate. *Compos. Struct.* **2004**, *63*, 115–122. [CrossRef]

35. Xiang, S.; Jiang, S.X.; Bi, Z.Y.; Jin, Y.X.; Yang, M.S. A nth-order meshless generalization of Reddy's third-order shear deformation theory for the free vibration on laminated composite plates. *Compos. Struct.* **2011**, *93*, 299–307. [CrossRef]